THE JOURNAL OF PHYSICAL CHEMISTRY Letters

pubs.acs.org/JPCL Letter

Thermodynamic Cost, Speed, Fluctuations, and Error Reduction of Biological Copy Machines

Yonghyun Song and Changbong Hyeon*

Cite This: *J. Phys. Chem. Lett.* 2020, 11, 3136−3143 Read Online

ACCESS | Metrics & More | Article Recommendations | Supporting Information

ABSTRACT: Due to large fluctuations in cellular environments, transfer of information in biological processes without regulation is error-prone. The mechanistic details of error-reducing mechanisms in biological copying processes have been a subject of active research; however, how error reduction of a process is balanced with its thermodynamic cost and dynamical properties remain largely unexplored. Here, we study the error reducing strategies in light of the recently discovered thermodynamic uncertainty relation (TUR) that sets a physical bound to the cost-precision trade-off for dissipative processes. We found that the two representative copying processes, DNA replication by the exonuclease-deficient T7 DNA polymerase and mRNA translation by the *E. coli* ribosome, reduce the error rates to biologically acceptable levels while also optimizing the processes close to the physical limit dictated by TUR.

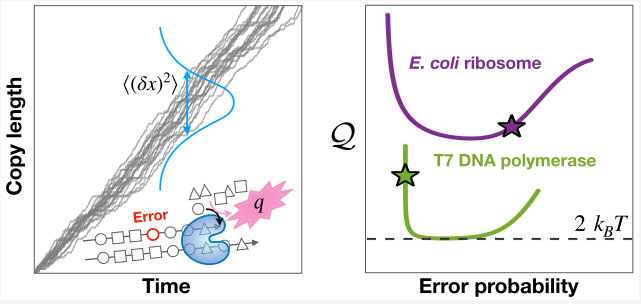

Biological copying processes, which include DNA replication, transcription, and translation, have evolved error-reducing mechanisms to faithfully transmit information in the genetic code. In their seminal papers in the 1970s, Hopfield and Ninio[1,2] proposed the *kinetic proofreading mechanism* to show that the energy-burning action of the mechanism can reduce the error rate. Shortly after, Bennett showed that the difference between kinetic barriers involving the incorporation of correct and incorrect substrates could be capitalized on to reduce the error rate under nonequilibrium chemical driving forces.[3] Despite differences in their mechanistic details, both models share a common feature that the reduction of copying error incurs free energy cost. Since these pioneering works, there have been a number of studies devoted to understanding the relation between the error reduction, speed, and energy consumption not only in the biological copying processes[4−9] but also in more general biochemical networks, including those related to sensory adaptation, circadian rhythm, and metabolic control.[10−15]

Besides the faithful transmission of genetic information, the primary goal of biological copying processes is to generate biomass in the forms of DNA, RNA, and proteins. Intuitively, however, error reduction comes at the cost of energy dissipation or slowing down of the process. Furthermore, fluctuations in biomass synthesis, which concomitantly increase with heat dissipation for Michaelis−Menten type processes,[16] also have to be suppressed below a biologically acceptable level. For instance, DNA replication in early fly embryogenesis occurs at high speed with exquisite precision; a modest change of 10% in replication timing could be lethal.[17] Similarly, for translation, it is well-known that cells must express genes at the right protein copy number for optimal function in a given environment;[18−20] regulatory mechanisms are developed to suppress the copy number fluctuation in gene expression.[21] How biological processes balance these conflicting requirements is a fundamental subject to explore. To address such an issue, the recently developed *thermodynamic uncertainty relation* (TUR),[22] which offers a quantitative bound for dissipative processes at nonequilibrium steady states (NESS), is well suited.

TUR expresses the trade-off between the thermodynamic cost and uncertainty of dynamical processes in NESS and specifies its physical bound as follows:

$$\mathcal{Q} = q(t)\,\epsilon_X{}^2(t) \geq 2k_BT \tag{1}$$

This form of TUR holds for most biological processes that can be represented either by stochastic jump processes on a kinetic network or by overdamped Langevin dynamics,[23−26] though extensions to more general conditions, which adjust the lower bound of the original relation, have also been discussed in recent years.[14,27−34] Briefly, $\epsilon_X(t) \equiv \sqrt{\langle \delta X(t)^2\rangle}/\langle X(t)\rangle$ is a relative uncertainty (or error) in an output observable $X(t)$ that best represents the dynamic process at time t, and $q(t)$

Received: February 19, 2020
Accepted: March 31, 2020
Published: March 31, 2020

https://dx.doi.org/10.1021/acs.jpclett.0c00545
J. Phys. Chem. Lett. 2020, 11, 3136−3143

denotes the thermodynamic cost or heat dissipation in generating the dynamic trajectory. The inequality in eq 1 allows one to quantitatively assess the physical limit to the precision that a dynamical process can maximize for a given amount of dissipation. Recently, $2k_BT/\mathcal{Q}$, which is bounded between 0 and 1, was suggested to quantify the "transport efficiency" of molecular motors.[25] When $\mathcal{Q}$ is written in the form of $\mathcal{Q} = \dot{q}(t)(2D/V^2)$ with D and V being the diffusivity and velocity of a molecular motor, the motor characterized with a small $\mathcal{Q}$ can be interpreted as an efficient cargo transporter, because it transports cargos with high velocity ($V \sim \langle X(t)\rangle/t$), small fluctuation ($D \sim \langle \delta X(t)^2\rangle/2t$), but with small dissipation rate ($\dot{q}$).[35] Biosynthetic reactions that are efficient in suppressing fluctuations in product formation can also be characterized by small $\mathcal{Q}$.

This work is organized into four parts. (i) We first introduce the basics of biological copying processes by reviewing the two distinct error reducing strategies by Bennett[3] and Hopfield.[1] (ii) We evaluate the error rate and $\mathcal{Q}$ of the replication process by the exonuclease-deficient T7 DNA polymerase, a model process reminiscent of the kinetic discrimination mechanism by Bennett. (iii) We analyze a model of mRNA translation where both Bennett's kinetic discrimination and Hopfield's kinetic proofreading are employed to lower the error rate and calculate $\mathcal{Q}$ for translating a codon into a polypeptide chain. (vi) Lastly, we consider a more realistic model of mRNA translation that explicitly accounts for 42 types of aa-tRNA and show that kinetic proofreading can suppress the fluctuation in the rate of polypeptide production.

Error Reducing Mechanisms by Bennett and Hopfield. We briefly describe the two representative error reducing mechanisms, one by Bennett and the other by Hopfield. In a nutshell, the essence of the two mechanisms is that the energy-dissipating enzyme reaction endows the biological copy machines with the power to discriminate correct substrates from incorrect ones. Illustrated in Figure 1A is an exemplary biological copying process where information on DNA sequence is copied by the DNA polymerase.

When the average reaction currents along the kinetic path associated with correct and incorrect substrate incorporation to the copy strand are defined as $\langle J^c\rangle$ and $\langle J^i\rangle$, respectively, the error probability, which will be discussed throughout this paper, is given by the ratio of two reaction currents

$$\eta = \frac{\langle J^i\rangle}{\langle J^c\rangle + \langle J^i\rangle} \tag{2}$$

Error reducing strategies of biological copying processes are at work to minimize η to a level acceptable for the survival of an organism.

The mechanism of the Bennett model (Figure 1)[3] uses the chemical potential of substrates, whose concentrations are kept out of equilibrium ($|\Delta\mu| \gg |\Delta\mu_{eq}|$), as the free energy drive. In the model, correct and incorrect substrates are *kinetically discriminated* with different kinetic barriers, but without having to have a difference in binding stabilities of the two substrate types. The average reaction currents, $\langle J^i\rangle$ and $\langle J^c\rangle$, are the function of the rate constants as well as the steady state populations (see eqs S2 and S3). At equilibrium, however, $\langle J^c\rangle = \langle J^i\rangle = 0$, and the error rate ($f = \langle J^i\rangle/\langle J^c\rangle$) is solely determined by the ratio of equilibrium binding probabilities to the copying system ($f_0 = 1$), so that $\eta_{eq} = f_0/(1 + f_0) = {}^1/_2$. In contrast, at the limit of large free energy drive ($|\Delta\mu| \to \infty$), the error probability converges to $\eta_0 = 1/(1 + e^{\beta\delta})$, which is solely determined by the difference between the kinetic barriers for substrate binding, $\beta\delta$, with $\beta = 1/k_BT$ being the inverse temperature. Thus, as long as $\delta > 0$, the mechanism can reduce the value of η from η_{eq} to η_0 at the expense of the free energy drive. See the Supporting Information text for the generalization of Bennett model where the equilibrium error rate is given by $f_0 = e^{-\beta\Delta\mu_i}/e^{-\beta\Delta\mu}$.

Meanwhile, the original Hopfield model[1] (see Figure 1B) assumes that the binding rates (**E** + **C** → **EC** or **E** + **I** → **EI** in Figure 1B) for the correct and incorrect substrates are identical ($k^c_{on}[c] = k^i_{on}[i]$). In discriminating correct substrates from incorrect ones, the mechanism takes advantage of the

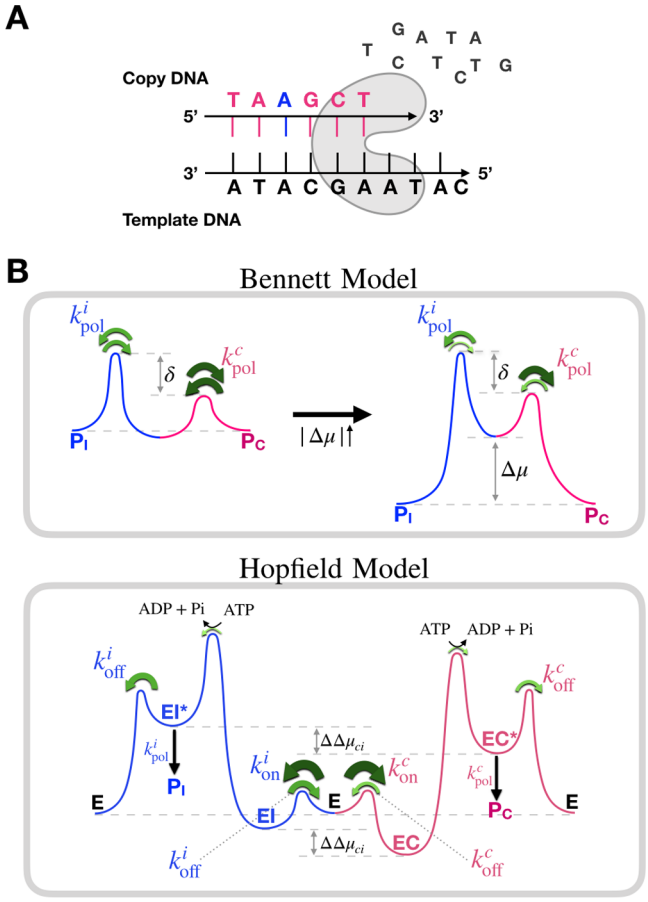

Figure 1. Error reducing mechanisms of Bennett and Hopfield. (A) Cartoon illustrating a biological copying process using DNA replication. When the sequence of template DNA is copied, complementary (correct, *c*) or noncomplementary (incorrect, *i*) nucleotide can be incorporated into the copy DNA. (B) (Top) Schematic of the Bennett model.[3] Substrates are polymerized through a one-step enzyme reaction. Energetic input in the form of the chemical potential of the substrates ($\Delta\mu$) leads to a larger current of correct substrate incorporation and reduces the error probability. (Bottom) Schematic of the Hopfield model.[1] The substrates are polymerized through a three-state kinetic mechanism with intermediate states **E**, **EC**, and **EC*** for correct substrate, or **E**, **EI**, and **EI*** for incorrect substrate. The reactions **EC** → **EC*** and **EI** → **EI***, which expend the chemical energy of ATP hydrolysis, are effectively irreversible. This allows the copy process to select against the incorrect substrate through two chances of facilitated unbinding, thereby reducing the error probability. For both schematics, the thickness and color of the arrows represent the relative magnitude of the respective rate constants.

https://dx.doi.org/10.1021/acs.jpclett.0c00545
J. Phys. Chem. Lett. 2020, 11, 3136−3143

facilitated unbinding of incorrect substrate from the copying system twice along the reaction path (**EI** → **E** + **I** and **EI*** → **E** + **I** in Figure 1B, bottom), assisted by the extra free energy from molecular fuel consumption (GTP or ATP hydrolysis), which renders the reaction paths **EC** → **EC*** and **EI** → **EI*** effectively irreversible. The substrates complementary to the template polymer sequence are more likely to be polymerized, whereas the preferential unbinding of incorrect substrates from the copying complex end up with expending the energy for *proofreading*, giving rise to the futile cycle. The mechanism of Hopfield model, called the *kinetic proofreading mechanism*, reduces the error rate from f_0 down to f_0^2.[1]

Real biological copying processes modify or combine the above two error-reducing strategies. More details on the different types of error reducing strategies and their combined effects can be found in refs 36 and 37.

Kinetic Discrimination of dNTP by the T7 DNA Polymerase. The DNA polymerase, in the absence of exonuclease activity, is an enzyme that adapts the kinetic discrimination mechanism to reduce errors in replication.[5,38,42] In its simplest form, the replication dynamics of DNA polymerases can be represented by a double-cyclic reversible three-state network consisting of two topologically identical subcycles for the incorporation of correct and incorrect nucleotides (Figure 2A). Following the binding of the substrate (dNTP) ([(1) ⇌ (2)]), the polymerase on DNA undergoes conformational change ([(2) ⇌ (3)]). Finally, the effectively irreversible polymerization associated with dNTP incorporation ([(3) ⇌ (1)]) with $k^c_{pol} \gg k^c_{dep}$ and $k^i_{pol} \gg k^i_{dep}$, completes the kinetic cycle. The free energy difference between the binding of correct and incorrect nucleotides is approximately $\approx 5\ k_BT$,[43] which implies that the error probability at equilibrium is $\eta_{eq} \approx 7 \times 10^{-3}$. In the presence of a nonequilibrium drive, the conditions of $k^c_{conf,f} \gg k^i_{conf,f}$ and $k^c_{pol} \gg k^i_{pol}$, engendering much larger reaction current along $\mathbf{E}^{(1)} \rightleftharpoons \mathbf{c}^{(2)} \rightleftharpoons \mathbf{c}^{(3)} \rightleftharpoons \mathbf{E}^{(1)}$ than that along $\mathbf{E}^{(1)} \rightleftharpoons \mathbf{i}^{(2)} \rightleftharpoons \mathbf{i}^{(3)} \rightleftharpoons \mathbf{E}^{(1)}$, allows DNA polymerases to reduce η below η_{eq}.[38,42]

As the total reaction current of polymerization, $\langle J_{pol}\rangle = \langle J^c_{pol}\rangle + \langle J^i_{pol}\rangle$, is a natural output observable accessible, for instance, in single molecule experiments,[44−46] we calculate $\mathcal{Q}$ of DNA replication as (see eq 1 and Methods)

$$\mathcal{Q} = \mathcal{A}\frac{\langle \delta J_{pol}{}^2\rangle}{\langle J_{pol}\rangle} \tag{3}$$

Alternatively, one could conceive choosing only the current of correct sequence incorporation, J^c_{pol}, as the output observable; however, unlike that of J_{pol}, the measurement of J^c_{pol} requires explicit knowledge of the DNA sequence being synthesized, which is not readily accessible to an experimental observer. As long as η is small, it is expected that $\langle J^c_{pol}\rangle \approx \langle J_{pol}\rangle$, and $\langle(\delta J^c_{pol})^2\rangle \approx \langle(\delta J_{pol})^2\rangle$; thus, choosing J^c_{pol} as the output observable instead of J_{pol} does not significantly alter the value of $\mathcal{Q}$.

The free energy cost for a single step of polymerization (affinity, $\mathcal{A}$) can be written as

$$\begin{aligned}\beta\mathcal{A} &= -\beta[(1-\eta)\Delta\mu_c + \eta\Delta\mu_i] - \eta\ln\eta - (1-\eta)\ln(1-\eta)\\ &\equiv -\beta\Delta\mu + I\end{aligned} \tag{4}$$

where $\Delta\mu_c$ and $\Delta\mu_i$ are the chemical potential difference along the correct and incorrect and polymerization cycles, respectively. $\beta\mathcal{A}$ can be decomposed into the free energy gain ($-\beta\Delta\mu$) and the Shannon-entropy (I) arising from the chance of incorporating correct versus incorrect monomers in the copy strand. It is noteworthy that although $I \le I_{max}$ (=ln 2) is usually small compared to $-\beta\Delta\mu$, it represents a fundamental thermodynamic property associated with stochastic copying processes (see eq S21).[47]

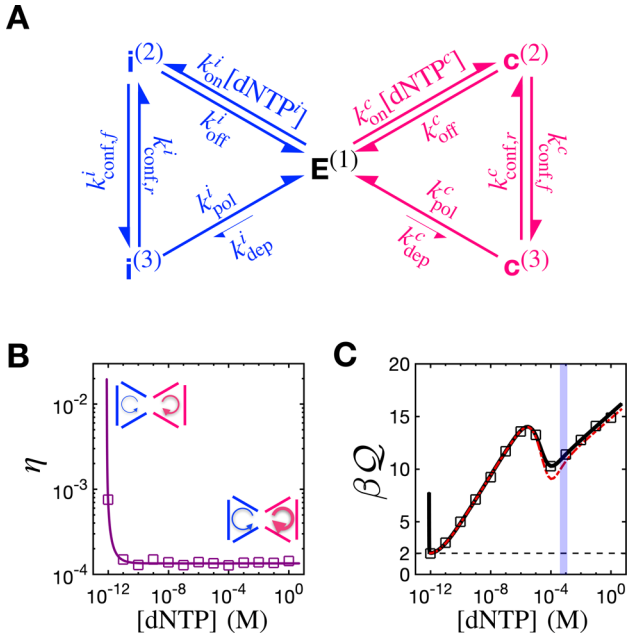

Figure 2. Error reduction of DNA replication by the exonuclease-deficient T7 DNA polymerase. (A) Kinetic network for the dynamics of DNA polymerase.[38] [dNTP^c] and [dNTP^i] are the concentration of the correct and incorrect nucleotides, respectively, where [dNTP^i] = 3[dNTP^c] holds from the assumption that all four substrates are present at identical concentrations. (B) Error probability (η) as a function of [dNTP] = [dNTP^c] + [dNTP^i]. With increasing [dNTP], relatively more reaction current flows in the subcycle associated with correct nucleotide incorporation. (C) $\mathcal{Q}$ of T7 DNA polymerase as functions of [dNTP]. The dash-dotted red line represents $\mathcal{Q}$ of an analogously defined unicyclic network with rate constants corresponding to the correct nucleotide incorporation pathway. The range of dNTP concentrations in *E. coli* is demarcated with the purple shade.[39−41] For (B) and (C), the data points (squares) represent results from stochastic simulations using the Gillespie algorithm (see the Supporting Information). See Figure S5 for other related dynamical properties.

We explore how $\mathcal{Q}$ is affected when the dNTP concentration ([dNTP]), which serves as a proxy for the chemical potential drive ($-\beta\Delta\mu$ in eq S10), increases. We assume that the four types of dNTPs (A, G, C, T) are maintained in solution at equal concentrations and use experimentally determined kinetic rates of the exonuclease-deficient T7 DNA polymerase to calculate η and $\mathcal{Q}$ (see Table S1).[38] With increasing [dNTP], the reaction current flows predominantly in one of the subcycles ($\langle J^c_{pol}\rangle \gg \langle J^i_{pol}\rangle$), and η decreases monotonically to values consistent with experimental measurements[5,48] (Figure 2B); by contrast, $\mathcal{Q}$ displays nonmonotonic variation (Figure 2C). For $\mathcal{Q}$, two minima are identified, one at $\mathcal{Q} \approx 2k_BT$, and the other at $\mathcal{Q} \approx 10k_BT$ ([dNTP] ≈ 100 μM), suggesting a complex interplay between the dissipation, current, and the current fluctuation. The suboptimal value of $\mathcal{Q}$ with respect to substrate concentration was also observed in models of transport motors.[35] Notably, the latter minimum is

https://dx.doi.org/10.1021/acs.jpclett.0c00545
J. Phys. Chem. Lett. 2020, 11, 3136−3143

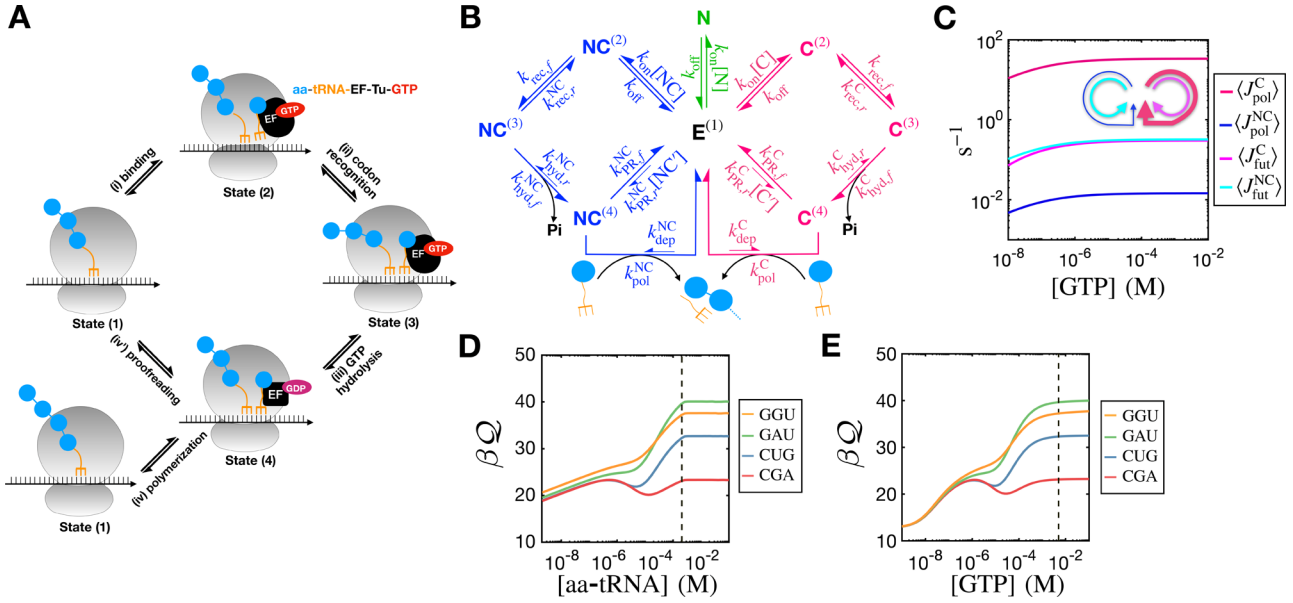

Figure 3. mRNA translation. (A)(B) Schematics of the catalytic cycle of the *E. coli* ribosome. In (B), $C^{(i)}$ and $NC^{(i)}$ (i = 2, 3, 4) represent intermediate states of the cognate and near-cognate aa-tRNA incorporation pathway. The state N represents the binding of the noncognate aa-tRNA. [C], [NC], and [N] represent the concentration of the cognate, near-cognate, and noncognate ternary complex substrate, (aa-tRNA)-(EF-Tu)-GTP, respectively. [C′] and [NC′] represent the concentration of the cognate and near-cognate (aa-tRNA)-(EF-Tu)-GDP, respectively. (C) Currents along the kinetic cycles as a function of [GTP] for codon CUG. The thickness of the lines in the inset schematic represents the relative magnitude of the reaction currents: $\langle J^{C}_{pol}\rangle \gg \langle J^{NC}_{fut}\rangle \gtrsim \langle J^{C}_{fut}\rangle \gg \langle J^{NC}_{pol}\rangle$. (D) $\mathcal{Q}$ as a function of [aa-tRNA]. (E) $\mathcal{Q}$ as a function of [GTP]. For (D) and (E), the dotted black line represents the cellular concentration in *E. coli*. See Figure S6 for other related dynamical properties.

found near the range of the *in vivo* [dNTP] in *E. coli* (430−1200 μM[39−41]) (Figure 2C).

To understand the nature of the two minima of $\mathcal{Q}$, we calculated $\mathcal{Q}$ of an analogously defined unicyclic three-state model with kinetic rates identical to those of the correct nucleotide incorporation cycle. The comparison between the $\mathcal{Q}$ of the two models suggests (i) the global minimum is formed near the DB condition [dNTP] $\approx \frac{k^{c}_{off}k^{c}_{conf,r}k^{c}_{dep}}{k^{c}_{on}k^{c}_{conf,f}k^{c}_{pol}}$ and (ii) the other minimum at [dNTP] $\approx$ 100 μM arises from the Michaelis−Menten (MM) type enzyme kinetics. For Michaelis−Menten enzyme reactions, $\mathcal{Q}$ is suboptimized when the substrate concentration is near the Michaelis−Menten constant ($[S] \approx K_m$), where the response of the reaction is maximal with respect to the logarithmic variation of substrate concentration (see the Supporting Information text).

Simplified Model of mRNA Translation. Since its introduction by Hopfield and Ninio,[1,2] kinetic proofreading has been the most extensively discussed error reducing strategy.[4,8,9,37] The proofreading reduces copy error by a resetting reaction that incurs an extra free energy. We study the effect of kinetic proofreading on $\mathcal{Q}$ by taking mRNA translation of the *E. coli* ribosome as our model system (see Figure 3).

The ribosome translates mRNA sequences into a polypeptide by reading *codons*, each consisting of three consecutive nucleic acids (Figure 3A). When an aa-tRNA of a "matching" codon binds to the ribosome-mRNA complex, the ribosome undergoes the reaction cycle for the *cognate* aa-tRNA incorporation (red cycle in Figure 3B). A *near-cognate* aa-tRNA with a single mismatch can also be incorporated, through a topologically identical but different kinetic pathway (blue cycle in Figure 3B). For aa-tRNAs with two or three mismatches, corresponding to noncognate aa-tRNAs, they can only interact with the ribosome-mRNA complex but cannot be incorporated into the reaction cycles (noncognate aa-tRNA binding is depicted with the reversible pathway colored in green in Figure 3B).[49,50]

Translation by the ribosome occurs via the following steps: (i) accommodation of an aa-tRNA to the ribosome-mRNA complex in the form of the (aa-tRNA)-(EF-Tu)-GTP complex [(1) ⇌ (2)]; (ii) the pairing of the codon-anticodon sequence [(2) ⇌ (3)]; (iii) GTP hydrolysis and the conformational change of EF-Tu [(3) ⇌ (4)]; (iv) a new peptide bond formation with the ribosome translocating to the next codon (k^{C}_{pol} and k^{NC}_{pol}) or (iv′) dissociation of (aa-tRNA)-(EF-Tu)-GDP complex from the ribosome (i.e., $k^{C}_{PR,f}$ and $k^{NC}_{PR,f}$). Both steps of (iv) and (iv′) reset the system back to the state (1) [(4) ⇌ (1)]. The cognate aa-tRNAs are differentiated from near-cognate aa-tRNAs mainly due to the faster rates of GTP hydrolysis and peptide bond formation ($k^{C}_{hyd,f} \gg k^{NC}_{hyd,f}$ and $k^{C}_{pol} \gg k^{NC}_{pol}$). The rates associated with tRNA binding, unbinding, and recognition are similar between the two. As a result, the reaction current of the cognate aa-tRNA incorporation is greater than that of the near-cognate aa-tRNA along the network depicted in Figure 3B. Because the incorporation current of noncognate aa-tRNA is effectively zero ($\langle J^{N}_{pol}\rangle = 0$), the error probability of the ribosome is $\eta = \langle J^{NC}_{pol}\rangle/(\langle J^{C}_{pol}\rangle + \langle J^{NC}_{pol}\rangle)$, where $\langle J^{C}_{pol}\rangle$ and $\langle J^{NC}_{pol}\rangle$ are the currents of cognate and near-cognate aa-tRNA incorporations, respectively.

Similar to DNA replication, the free energy cost for a single step of translation ($\mathcal{A}$) can be written as

$$\beta\mathcal{A} = -\beta\left[\Delta\mu_{pol} + \frac{\langle J_{fut}\rangle}{\langle J_{pol}\rangle}\Delta\mu_{fut}\right] - \eta\ln\eta - (1-\eta)\ln(1-\eta) \quad (5)$$

Here, $\Delta\mu_{fut}$ and $\Delta\mu_{pol}$ are the chemical potential difference along the futile and polymerization cycles, respectively (see the

https://dx.doi.org/10.1021/acs.jpclett.0c00545
J. Phys. Chem. Lett. 2020, 11, 3136−3143

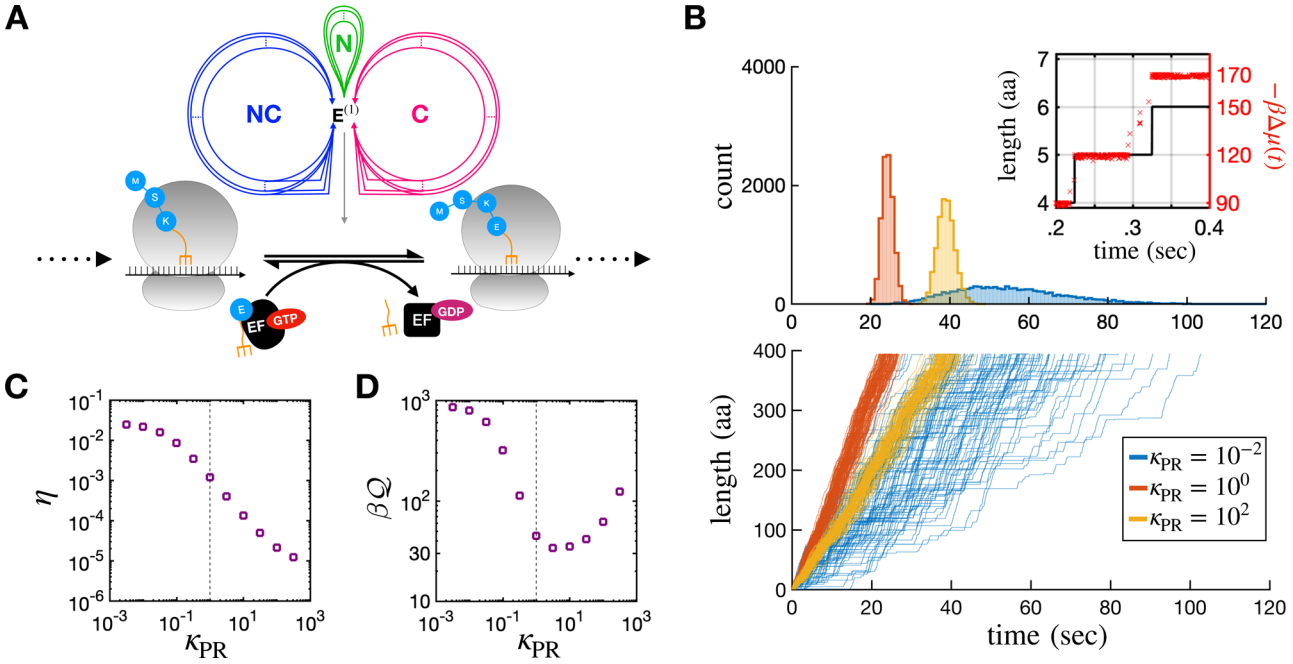

Figure 4. Reaction kinetics of translation with 42 aa-tRNA species. (A) Schematic of the translation of the *tufB* mRNA sequence into EF-Tu. For each reaction cycle, 42 different aa-tRNAs can bind to the apo state of the enzyme. Out of these, the cognate and near cognate aa-tRNAs can undergo the reaction cycle previously defined in Figure 3B. For more detail on the simulated reaction network, refer to the Supporting Information. (B) (Bottom) Ensemble of time traces ($N = 100$) generated from the numerics using Gillespie algorithm that simulates the mRNA translation (or the synthesis of the polypeptides consisting of 394 amino acids) at different values of κ_{PR}. (Top) Histogram of translation completion times. The inset shows a sample trajectory at the wild type condition ($\kappa_{PR} = 1$), at which a proofreading reaction occurs at around 0.3 s. The average dissipation from the process is shown with red crosses ($\Delta\mu(t)$). Whenever the proofreading takes place, the synthesis of polypeptide is stalled. (C) Error probability and (D) Q of TUR plotted against κ_{PR}. The dotted lines depict the wild type condition ($\kappa_{PR} = 1$).

Supporting Information for details). The kinetic proofreading uses extra energy in the form of GTP hydrolysis ($\Delta\mu_{fut}$), engendering futile cycles, and reduces η further than that by kinetic discrimination alone, the latter of which only capitalizes on the thermodynamic cost of polymerization ($\Delta\mu_{pol}$).

The dynamics of mRNA translation was examined as a function of the concentration of aa-tRNA and GTP by assuming that the ternary complex concentration was in pseudoequilibrium with respect to the concentration of its components, aa-tRNA, EF-Tu, GTP, and GDP (see the Supporting Information). With increasing [GTP], the polymerization current of all cycles increases while maintaining their relative magnitudes: $\langle J^{C}_{pol}\rangle \gg \langle J^{NC}_{fut}\rangle \gtrsim \langle J^{C}_{fut}\rangle \gg \langle J^{NC}_{pol}\rangle$ (Figure 3C). In other words, while most cognate aa-tRNAs that reach state $\mathbf{C}^{(4)}$ are polymerized, most of the near-cognate aa-tRNAs that reach state $\mathbf{NC}^{(4)}$ are rejected by the proofreading reaction.

For all codon types, η is nearly constant for a wide range of [aa-tRNA] and [GTP] (Figure S6A,E). In contrast, the shape of Q varies depending on the codon (Figure 3D,E). For most codons, Q increases monotonically with [aa-tRNA] and [GTP]. For codons CGA and CUG, Q has a local minimum at [aa-tRNA] $\approx$ 10 μM and [GTP] $\approx$ 10 μM. The distinguishing feature of the codons CGA and CUG is their high cognate to near-cognate aa-tRNA concentration ratios ([C]/[NC] $\approx$ 0.9 for CGA and [C]/[NC] $\approx$ 0.5 for CUG. Figure S7), which suggests that the local minimum of Q occurs when the contribution from the near-cognate incorporation pathway is relatively low. As seen in the case of T7 DNA polymerase (Figure 2C and Figure S5), the local minimum of Q (Figure 3D,E), if any, is identified at regions where the response of $\langle J_{pol}\rangle$ is large with respect to the logarithmic variation of [aa-tRNA] or [GTP] (Figure S6B,F).

Multicyclic Model of mRNA Translation. To address the mRNA translation in a more realistic fashion, we consider a multicyclic model that translates 42 species of aa-tRNAs into 20 different amino acids (Figure 4). For each codon, the 42 aa-tRNAs are grouped into cognate, near-cognate, and non-cognate types (Figure S7). Using the information on the concentration of 42 aa-tRNAs and the model illustrated in Figure 4A, we simulated the translation of the *tufB* mRNA sequence, which encodes for the $n_{aa} = 394$ amino acid EF-Tu, a highly abundant protein in *E. coli*[51] (Figure 4).

The dynamics arising from the multicyclic model are studied using an ensemble of trajectories generated from Gillespie simulations (Figure 4B). The total number of translational steps (N_{tln}) that complete the polymerization of the full amino-acid sequences varies from one realization to another. Selecting the completion time of translation ($\mathcal{T}$) as the output observable for each dynamic process, we define TUR of translation as

$$Q = [-\Delta\mu + \beta^{-1}I]\frac{\langle(\delta\mathcal{T})^2\rangle}{\langle\mathcal{T}\rangle^2} \tag{6}$$

where, similarly to all previous models, the dissipation has contributions from the free energy drive ($\Delta\mu$) and Shannon-entropy (I). Denoting the forward and reverse rate constants of each kinetic step by $k_{i,f}$ and $k_{i,r}$ for $i = 1, \ldots, N_{tln}$, we can compute the average free energy drive by $-\beta\Delta\mu = \langle\sum_{i=1}^{N_{tln}} \ln(k_{i,f}/k_{i,r})\rangle$, where $\langle\cdots\rangle$ denotes the average over the ensemble of 10^4 realizations. The entropic contribution can be

https://dx.doi.org/10.1021/acs.jpclett.0c00545
J. Phys. Chem. Lett. 2020, 11, 3136−3143

computed as $I = -\sum_{l=1}^{n_{aa}} \sum_{i_{aa}=1}^{20} \eta_{i_{aa}}^{l} \ln \eta_{i_{aa}}^{l}$ where $\eta_{i_{aa}}^{l}$ is the probability of incorporating one of the 20 types of amino acids, at the lth position.

Using the multicyclic model, we evaluated η and $\mathcal{Q}$ with respect to perturbations to the proofreading reaction, by considering a multiplication factor κ_{PR} to the original wild-type (WT) rate constants $k_{PR,f}^{C}$, $k_{PR,r}^{C}$, $k_{PR,f}^{NC}$, and $k_{PR,r}^{NC}$. Although the rate constants are not experimentally tunable parameters like [GTP], the cell can optimize them throughout the evolution by means of mutations to the ribosome, EF-Tu, and tRNA. This type of perturbative analysis can be used to decipher which feature of the reaction kinetics for mRNA translation is optimized in the cell (see the effect of other perturbations in Figure S8).

The WT level of proofreading gives rise to an average speed $\langle J_{pol} \rangle \approx 16$ aa/sec and error probability $\eta \approx 10^{-3}$ in our simulation, consistent with the experimental measurements.[52,53] While η decreases monotonically with κ_{PR}, $\mathcal{Q}$ is nonmonotonic with κ_{PR}, minimized near the wild type condition. At $\kappa_{PR} = 1$ we obtain $\mathcal{Q} \approx 45 k_B T$[54] (Figure 4D). For the given kinetic parameters from WT, $\mathcal{Q}$ is minimized to $\sim 30\ k_B T$ when the rates of proofreading is augmented by 5 fold. In a scenario of negligibly low proofreading ($\kappa_{PR} = 10^{-2}$), the completion times for the translation display a much broader distribution than that by the WT ($\kappa_{PR} = 1$). Thus, near the WT condition, proofreading can simultaneously improve the fidelity of translation and suppress the fluctuation of protein synthesis in an energetically efficient way.

Importantly, fluctuations in the completion time for mRNA translation can be critical, as it could in turn lead to significant variation in protein copy number. Thus, our results demonstrate that kinetic proofreading, an error reducing strategy, can also contribute to the energetically efficient control of protein levels.

Implications of the T7 DNA Polymerase model. In the wild type T7 DNA polymerase, the proofreading activity of the exonuclease further reduces η by 2 orders of magnitude.[55] In fact, in more complex systems like DNA replication of *E. coli*, the combination of the actions of DNA polymerase, exonuclease, and mismatch repair machineries achieves an error probability as small as $\eta \approx 10^{-10}$.[56] Although these extra components of DNA replication could in principle be included in our model,[3,57−59] general consensus on their kinetic network and measurement of kinetic rates are currently lacking. Thus, we focused on the simpler, yet still experimentally realizable, exonuclease-deficient T7 DNA polymerase, which has served as a useful tool for sequencing technologies and for biochemical studies of DNA polymerases.[38,60]

For the exonuclease-deficient T7 DNA polymerase, we found that $\mathcal{Q}$ is suboptimized near the physiological [dNTP]. Similarly, it has recently been discovered that in metabolic reactions, the physiological substrate concentrations are generally close to their respective K_m values.[61] A systems level analysis of yeast metabolism also showed that reaction currents of metabolism are generally self-regulated to the values at which their response to the change in substrate concentration is significant.[62] In light of our analysis of Michaelis−Menten enzyme reactions (see the section "Michaelis−Menten reactions" in the Supporting Information), the above-mentioned condition of metabolism is closely related with the condition of suboptimized $\mathcal{Q}$.

mRNA Translation Combines the Strategies of Kinetic Discrimination and Proofreading. The nonmonotonic variation of $\mathcal{Q}$ with κ_{PR} (Figure 4D) is not a feature of the original kinetic proofreading model, which lacks the forward kinetic discrimination (i.e., $\beta\delta = 0$). As the perturbative parameter κ_{PR} is increased, the error rate ($f = \langle J_{pol}^{i} \rangle / \langle J_{pol}^{c} \rangle$) is reduced to $f \gtrsim f_0^2 = e^{-2\beta(\Delta\mu_i - \Delta\mu_t)}$ (Figure S9A, blue line). Furthermore, in the original Hopfield model, the Fano factor (see eq 8) $\lambda \approx 1$ regardless of κ_{PR} (Figure S9D), which leads to $\mathcal{Q} \approx \mathcal{A}$, and a monotonically increasing $\mathcal{Q}$ with κ_{PR} (Figure S9C,E).

To introduce the kinetic discrimination to the Hopfield model, we consider a modified version, the associated kinetic constants of which satisfy the following relations with $\beta\delta > 0$:

$$e^{\beta\delta} = \frac{k_{on}^{c}}{k_{on}^{i}} = \frac{k_{hyd,f}^{c}}{k_{hyd,f}^{i}} = \frac{k_{pol}^{c}}{k_{pol}^{i}} = \frac{k_{PR,r}^{c}}{k_{PR,r}^{i}} \tag{7}$$

As expected, η decreases monotonically with $\beta\delta$ and κ_{PR} (Figure 5A). Qualitatively similar to mRNA translation, $\mathcal{Q}$ is

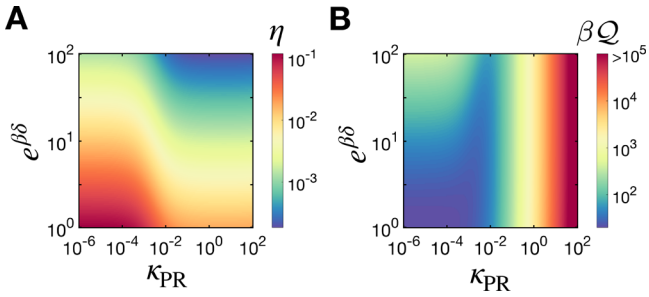

Figure 5. Modified Hopfield model with kinetic discrimination. (A) Error probability (η) and (B) $\mathcal{Q}$ with respect to variations in δ and κ_{PR} defined in the main text. The rate constants used to generate the plots are given in Table S3. See Figure S9 for other related dynamical properties plotted for $\beta\delta = 0$ and $\beta\delta = \ln 10$.

minimized over a certain range of κ_{PR} as long as $e^{\beta\delta} \gtrsim 10^{1}$ (Figure 5B and Figure S9E). Taken together with the modified Hopfield model, mRNA translation in *E. coli* balances the kinetic discrimination and proofreading, to attain low η and suboptimized $\mathcal{Q}$.

Optimality of the Speed and TUR in the E. coli Ribosome. Recent theoretical studies on mRNA translation by the ribosome[4,6] have observed that while the error probability is still far from its minimum, the WT value of the mean first translation time ($\langle \tau_{MFPT} \rangle$) is close to its minimum; and hence it was concluded that the *E. coli* ribosome is primarily optimized for speed. As far as the κ_{PR} dependencies of speed ($\langle J_{pol} \rangle \approx \langle \tau_{MFPT} \rangle^{-1}$) and η are concerned, our study points to the same finding (Figure S8). In fact, recent studies, which showed translational pausing caused protein misfolding, lend support to the significance of optimal codon translation speed.[63,64]

Fast codon translation speed, small fluctuations in total translation time, and low thermodynamic costs could be favorable characteristics of translation, all likely under evolutionary selection pressure;[65] however, not all of these requirements can be fulfilled simultaneously. In this aspect, of great significance is our finding that the TUR measure of *E. coli* ribosome ($\mathcal{Q} \approx 45 k_B T$) for the wild type condition is in the vicinity of its minimum with respect to κ_{PR} ($\sim 30\ k_B T$) (Figure 4D).

https://dx.doi.org/10.1021/acs.jpclett.0c00545
J. Phys. Chem. Lett. 2020, 11, 3136−3143

Significance of Small. $\mathcal{Q}$. The theoretical lower bound of TUR ($\mathcal{Q} = 2k_BT$) allows us to endow physical significance to the $\mathcal{Q}$ values obtained for the two essential copy machines ($\mathcal{Q} \approx 10k_BT$ for the T7 DNA polymerase and $\mathcal{Q} \approx 45k_BT$ for the *E. coli* ribosome). For instance, we can compare $\mathcal{Q}$ of copying enzymes to molecular clocks, in which TUR is defined with respect to the trade-off between the energetic cost and the uncertainty in the cycle duration. Marsland et al. have recently demonstrated that TUR of multiple types of biochemical oscillators severely underperform the $2k_BT$ bound.[14] For the circadian KaiABC oscillator system, $\beta\mathcal{Q} \gtrsim O(10^2)$. This either implies that the precision of cycle periodicity is the key priority over the energy expenditure, or that this synthetic biochemical cycle is not optimally designed under the constraint of TUR. In contrast, biological motors that transport cargo along cytoskeletal filaments display small $\beta\mathcal{Q}(\approx 7 - 15)$, simultaneously minimizing energetic costs, fluctuation, and maximizing speed.[35] Compared to biological motors harnessing the thermal fluctuations along with the ATP hydrolysis free energy, synthetic nanomachines,[66] which uses ∼eV UV-light source as the driving force, are expected to have much greater $\mathcal{Q}$ values. While the biological function of copying enzymes is to maintain low copying error, it is remarkable to discover that T7 DNA polymerase and *E. coli* ribosome are also working at conditions close to the theoretical bound dictated by the TUR.

METHODS

When the number of steps taken by the enzyme is selected as the output observable ($X(t) = n(t)$ in eq 1), TUR in eq 1 is modified to

$$\mathcal{Q} = q(t)\frac{\langle \delta n(t)^2 \rangle}{\langle n(t) \rangle^2} = \mathcal{A}\lambda \geq 2k_BT \tag{8}$$

where $\mathcal{A} = q(t)/\langle n(t) \rangle$ and $\lambda = \langle \delta n(t)^2 \rangle / \langle n(t) \rangle$ is the Fano factor of the copying process, which can also be written as $\lambda = \langle \delta J^2 \rangle / \langle J \rangle$.

ASSOCIATED CONTENT

Supporting Information

The Supporting Information is available free of charge at https://pubs.acs.org/doi/10.1021/acs.jpclett.0c00545.

Full details of Bennett and Hopfield models, TUR for reversible Michaelis−Menten reactions, mathematical expressions of η and $\mathcal{A}$ for general copying processes, stochastic simulations of DNA replication and mRNA translation, and the details associated with the model for mRNA translation by the *E. coli* ribosome (PDF)

AUTHOR INFORMATION

Corresponding Author

Changbong Hyeon − *Korea Institute for Advanced Study, Seoul 02455, Korea;* orcid.org/0000-0002-4844-7237; Email: hyeoncb@kias.re.kr

Author

Yonghyun Song − *Korea Institute for Advanced Study, Seoul 02455, Korea*

Complete contact information is available at: https://pubs.acs.org/10.1021/acs.jpclett.0c00545

Notes

The authors declare no competing financial interest.

ACKNOWLEDGMENTS

This work was supported by the KIAS Individual Grant No. CG067102 (Y.S.) and No. CG035003 (C.H.) at Korea Institute for Advanced Study. We thank the Center for Advanced Computation in KIAS for providing computing resources.

REFERENCES

(1) Hopfield, J. Kinetic Proofreading: A New Mechanism for Reducing Errors in Biosynthetic Processes Requiring High Specificity. *Proc. Natl. Acad. Sci. U. S. A.* **1974**, *71*, 4135−4139.

(2) Ninio, J. Kinetic amplification of enzyme discrimination. *Biochimie* **1975**, *57*, 587−595.

(3) Bennett, C. H. Dissipation-Error Tradeoff in Proofreading. *BioSystems* **1979**, *11*, 85−91.

(4) Banerjee, K.; Kolomeisky, A. B.; Igoshin, O. A. Elucidating interplay of speed and accuracy in biological error correction. *Proc. Natl. Acad. Sci. U. S. A.* **2017**, *114*, 5183−5188.

(5) Cady, F.; Qian, H. Open-system thermodynamic analysis of DNA polymerase fidelity. *Phys. Biol.* **2009**, *6*, 036011.

(6) Mallory, J. D.; Kolomeisky, A. B.; Igoshin, O. A. Trade-Offs between Error, Speed, Noise, and Energy Dissipation in Biological Processes with Proofreading. *J. Phys. Chem. B* **2019**, *123*, 4718−4725.

(7) Mellenius, H.; Ehrenberg, M. Transcriptional accuracy modeling suggests two-step proofreading by RNA polymerase. *Nucleic Acids Res.* **2017**, *45*, 11582−11593.

(8) Murugan, A.; Huse, D. A.; Leibler, S. Speed, dissipation, and error in kinetic proofreading. *Proc. Natl. Acad. Sci. U. S. A.* **2012**, *109*, 12034−12039.

(9) Rao, R.; Peliti, L. Thermodynamics of accuracy in kinetic proofreading: Dissipation and efficiency trade-offs. *J. Stat. Mech.: Theory Exp.* **2015**, *2015*, P06001.

(10) Cao, Y.; Wang, H.; Ouyang, Q.; Tu, Y. The free-energy cost of accurate biochemical oscillations. *Nat. Phys.* **2015**, *11*, 772−778.

(11) Hartich, D.; Barato, A. C.; Seifert, U. Nonequilibrium sensing and its analogy to kinetic proofreading. *New J. Phys.* **2015**, *17*, 055026.

(12) François, P.; Altan-Bonnet, G. The Case for Absolute Ligand Discrimination: Modeling Information Processing and Decision by Immune T Cells. *J. Stat. Phys.* **2016**, *162*, 1130−1152.

(13) Lan, G.; Tu, Y. The cost of sensitive response and accurate adaptation in networks with an incoherent type-1 feed-forward loop. *J. R. Soc., Interface* **2013**, *10*, 20130489.

(14) Marsland, R.; Cui, W.; Horowitz, J. M. The thermodynamic uncertainty relation in biochemical oscillations. *J. R. Soc., Interface* **2019**, *16*, 20190098.

(15) Qian, H.; Beard, D. A. Metabolic futile cycles and their functions: A systems analysis of energy and control. *IEE Proceedings: Systems Biology* **2006**, *153*, 192−200.

(16) Hwang, W.; Hyeon, C. Quantifying the Heat Dissipation from Molecular Motor's Transport Properties in Nonequilibrium Steady States. *J. Phys. Chem. Lett.* **2017**, *8*, 250−256.

(17) Djabrayan, N. J.; Smits, C. M.; Krajnc, M.; Tomer, S.; Yamada, S.; Lemon, W. C.; Keller, P. J.; Rushlow, C. A.; Shvartsman, S. Y. Metabolic Regulation of Developmental Cell Cycles and Zygotic Transcription. *Curr. Biol.* **2019**, *29*, 1193.

(18) Dekel, E.; Alon, U. Optimality and evolutionary tuning of the expression level of a protein. *Nature* **2005**, *436*, 588−592.

(19) Scott, M.; Klumpp, S.; Mateescu, E. M.; Hwa, T. Emergence of robust growth laws from optimal regulation of ribosome synthesis. *Mol. Syst. Biol.* **2014**, *10*, 747.

(20) Li, G.-W.; Burkhardt, D.; Gross, C.; Weissman, J. S. Quantifying absolute protein synthesis rates reveals principles underlying allocation of cellular resources. *Cell* **2014**, *157*, 624−35.

(21) Fraser, H. B.; Hirsh, A. E.; Giaever, G.; Kumm, J.; Eisen, M. B. Noise minimization in eukaryotic gene expression. *PLoS Biol.* **2004**, *2*, e137.
(22) Barato, A. C.; Seifert, U. Thermodynamic Uncertainty Relation for Biomolecular Processes. *Phys. Rev. Lett.* **2015**, *114*, 158101.
(23) Gingrich, T. R.; Horowitz, J. M.; Perunov, N.; England, J. L. Dissipation Bounds All Steady-State Current Fluctuations. *Phys. Rev. Lett.* **2016**, *116*, 120601.
(24) Hyeon, C.; Hwang, W. Physical Insight into the Thermodynamic Uncertainty Relation Using Brownian Motion in Tilted Periodic Potentials. *Phys. Rev. E: Stat. Phys., Plasmas, Fluids, Relat. Interdiscip. Top.* **2017**, *96*, 012156.
(25) Dechant, A.; Sasa, S.-i. Entropic bounds on currents in Langevin systems. *Phys. Rev. E: Stat. Phys., Plasmas, Fluids, Relat. Interdiscip. Top.* **2018**, *97*, 062101.
(26) Pigolotti, S.; Neri, I.; Roldán, É.; Jülicher, F. Generic Properties of Stochastic Entropy Production. *Phys. Rev. Lett.* **2017**, *119*, 140604.
(27) Lee, S.; Hyeon, C.; Jo, J. Thermodynamic uncertainty relation of interacting oscillators in synchrony. *Phys. Rev. E: Stat. Phys., Plasmas, Fluids, Relat. Interdiscip. Top.* **2018**, *98*, 032119.
(28) Horowitz, J. M.; Gingrich, T. R. Proof of the finite-time thermodynamic uncertainty relation for steady-state currents. *Phys. Rev. E: Stat. Phys., Plasmas, Fluids, Relat. Interdiscip. Top.* **2017**, *96*, 020103.
(29) Brandner, K.; Hanazato, T.; Saito, K. Thermodynamic bounds on precision in ballistic multiterminal transport. *Phys. Rev. Lett.* **2018**, *120*, 090601.
(30) Barato, A. C.; Chetrite, R.; Faggionato, A.; Gabrielli, D. Bounds on current fluctuations in periodically driven systems. *New J. Phys.* **2018**, *20*, 103023.
(31) Chun, H.-M.; Fischer, L. P.; Seifert, U. Effect of a magnetic field on the thermodynamic uncertainty relation. *Phys. Rev. E: Stat. Phys., Plasmas, Fluids, Relat. Interdiscip. Top.* **2019**, *99*, 042128.
(32) Hasegawa, Y.; Van Vu, T. Fluctuation theorem uncertainty relation. *Phys. Rev. Lett.* **2019**, *123*, 110602.
(33) Timpanaro, A. M.; Guarnieri, G.; Goold, J.; Landi, G. T. Thermodynamic Uncertainty Relations from Exchange Fluctuation Theorems. *Phys. Rev. Lett.* **2019**, *123*, 090604.
(34) Horowitz, J. M.; Gingrich, T. R. Thermodynamic uncertainty relations constrain non-equilibrium fluctuations. *Nat. Phys.* **2020**, *16*, 15−20.
(35) Hwang, W.; Hyeon, C. Energetic Costs, Precision, and Transport Efficiency of Molecular Motors. *J. Phys. Chem. Lett.* **2018**, *9*, 513−520.
(36) Sartori, P.; Pigolotti, S. Kinetic versus energetic discrimination in biological copying. *Phys. Rev. Lett.* **2013**, *110*, 188101.
(37) Pigolotti, S.; Sartori, P. Protocols for Copying and Proofreading in Template-Assisted Polymerization. *J. Stat. Phys.* **2016**, *162*, 1167−1182.
(38) Tsai, Y. C.; Johnson, K. A. A new paradigm for DNA polymerase specificity. *Biochemistry* **2006**, *45*, 9675−9687.
(39) Bochner, B. R.; Ames, B. N. Complete analysis of cellular nucleotides by two-dimensional thin layer chromatography. *J. Biol. Chem.* **1982**, *257*, 9759−9769.
(40) Buckstein, M. H.; He, J.; Rubin, H. Characterization of nucleotide pools as a function of physiological state in Escherichia coli. *J. Bacteriol.* **2008**, *190*, 718−726.
(41) Schaaper, R. M.; Mathews, C. K. Mutational consequences of dNTP pool imbalances in E. coli. *DNA Repair* **2013**, *12*, 73−79.
(42) Johnson, K. A. The kinetic and chemical mechanism of high-fidelity DNA polymerases. *Biochim. Biophys. Acta, Proteins Proteomics* **2010**, *1804*, 1041−1048.
(43) Goodman, M. F. Hydrogen bonding revisited: Geometric selection as a principal determinant of DNA replication fidelity. *Proc. Natl. Acad. Sci. U. S. A.* **1997**, *94*, 10493−10495.
(44) Abbondanzieri, E. A.; Greenleaf, W. J.; Shaevitz, J. W.; Landick, R.; Block, S. M. Direct observation of base-pair stepping by RNA polymerase. *Nature* **2005**, *438*, 460.
(45) Wen, J.-D.; Lancaster, L.; Hodges, C.; Zeri, A.-C.; Yoshimura, S. H.; Noller, H. F.; Bustamante, C.; Tinoco, I. Following translation by single ribosomes one codon at a time. *Nature* **2008**, *452*, 598.
(46) Kaiser, C. M.; Goldman, D. H.; Chodera, J. D.; Tinoco, I.; Bustamante, C. The ribosome modulates nascent protein folding. *Science* **2011**, *334*, 1723−1727.
(47) Sartori, P.; Pigolotti, S. Thermodynamics of Error Correction. *Phys. Rev. X* **2015**, *5*, 041039.
(48) Kunkel, T. A.; Patel, S. S.; Johnson, K. A. Error-prone replication of repeated DNA sequences by T7 DNA polymerase in the absence of its processivity subunit. *Proc. Natl. Acad. Sci. U. S. A.* **1994**, *91*, 6830−6834.
(49) Dong, H.; Nilsson, L.; Kurland, C. G. Co-variation of tRNA abundance and codon usage in Escherichia coli at different growth rates. *J. Mol. Biol.* **1996**, *260*, 649−663.
(50) Wohlgemuth, I.; Pohl, C.; Mittelstaet, J.; Konevega, A. L.; Rodnina, M. V. Evolutionary optimization of speed and accuracy of decoding on the ribosome. *Philos. Trans. R. Soc., B* **2011**, *366*, 2979−2986.
(51) Ishihama, Y.; Schmidt, T.; Rappsilber, J.; Mann, M.; Harlt, F. U.; Kerner, M. J.; Frishman, D. Protein abundance profiling of the Escherichia coli cytosol. *BMC Genomics* **2008**, *9*, 102.
(52) Bouadloun, F.; Donner, D.; Kurland, C. Codon-specific missense errors in vivo. *EMBO J.* **1983**, *2*, 1351−1356.
(53) Young, R.; Bremer, H. Polypeptide chain elongation rate in Escherichia coli B/r as a function of growth rate. *Biochem. J.* **1976**, *160*, 185−194.
(54) Piñeros, W. D.; Tlusty, T. Kinetic proofreading and the limits of thermodynamic uncertainty. *Phys. Rev. E: Stat. Phys., Plasmas, Fluids, Relat. Interdiscip. Top.* **2020**, *101*, 022415.
(55) Donlin, M. J.; Patel, S. S.; Johnson, K. A. Kinetic Partitioning between the Exonuclease and Polymerase Sites in DNA Error Correction. *Biochemistry* **1991**, *30*, 538−546.
(56) Schaaper, R. M. Base selection, proofreading, and mismatch repair during DNA replication in Escherichia coli. *J. Biol. Chem.* **1993**, *268*, 23762−23765.
(57) Banerjee, K.; Kolomeisky, A. B.; Igoshin, O. A. Elucidating Interplay of Speed and Accuracy in Biological Error Correction. *Proc. Natl. Acad. Sci. U. S. A.* **2017**, *114*, 5183−5188.
(58) Gaspard, P. Kinetics and thermodynamics of DNA polymerases with exonuclease proofreading. *Phys. Rev. E: Stat. Phys., Plasmas, Fluids, Relat. Interdiscip. Top.* **2016**, *93*, 042420.
(59) Hoekstra, T. P.; Depken, M.; Lin, S. N.; Cabanas-Danés, J.; Gross, P.; Dame, R. T.; Peterman, E. J.; Wuite, G. J. Switching between Exonucleolysis and Replication by T7 DNA Polymerase Ensures High Fidelity. *Biophys. J.* **2017**, *112*, 575−583.
(60) Zhu, B. Bacteriophage T7 DNA polymerase-sequenase. *Front. Microbiol.* **2014**, *5*, 181.
(61) Park, J. O.; Rubin, S. A.; Xu, Y.-F.; Amador-Noguez, D.; Fan, J.; Shlomi, T.; Rabinowitz, J. D. Metabolite concentrations, fluxes and free energies imply efficient enzyme usage. *Nat. Chem. Biol.* **2016**, *12*, 482−489.
(62) Hackett, S. R.; Zanotelli, V. R.; Xu, W.; Goya, J.; Park, J. O.; Perlman, D. H.; Gibney, P. A.; Botstein, D.; Storey, J. D.; Rabinowitz, J. D. Systems-level analysis of mechanisms regulating yeast metabolic flux. *Science* **2016**, *354*, aaf2786.
(63) Nedialkova, D. D.; Leidel, S. A. Optimization of codon translation rates via tRNA modifications maintains proteome integrity. *Cell* **2015**, *161*, 1606−1618.
(64) Trovato, F.; O'Brien, E. P. Fast protein translation can promote co-and posttranslational folding of misfolding-prone proteins. *Biophys. J.* **2017**, *112*, 1807−1819.
(65) Ilker, E.; Hinczewski, M. Modeling the Growth of Organisms Validates a General Relation between Metabolic Costs and Natural Selection. *Phys. Rev. Lett.* **2019**, *122*, 238101.
(66) Kudernac, T.; Ruangsupapichat, N.; Parschau, M.; Maciá, B.; Katsonis, N.; Harutyunyan, S. R.; Ernst, K.-H.; Feringa, B. L. Electrically driven directional motion of a four-wheeled molecule on a metal surface. *Nature* **2011**, *479*, 208.

https://dx.doi.org/10.1021/acs.jpclett.0c00545
J. Phys. Chem. Lett. 2020, 11, 3136−3143